Optica Applicata, Vol. XXXV, No. 3, 2005

Optimization of multi quantum well solar cell

JOANNA PRAŻMOWSKA*, RYSZARD KORBUTOWICZ

Faculty of Microsystem Electronics and Photonics, Wrocław University of Technology, Janiszewskiego 11/12, 50-372 Wrocław, Poland

*Corresponding author: J. Prażmowska, Joanna.Prazmowska@pwr.wroc.pl

Quantum well solar cell with GaAs wells and $Al_xGa_{1-x}As$ barriers was optimized. Particular emphasis was placed on enhancing the efficiency. Open-circuit voltage, short-circuit current density, fill factor have been also optimized. Many simulations of various structures were carried out. The conversion efficiency exceeding 27% was obtained. The algorithm of structures optimization that gives comprehensive information about solar cells parameters in a short time was shown. Spectral characteristics, efficiency of energy conversion as a function of light concentration, temperature and the geometrical and materials parameters of the solar cells structures were determined. These results are compared with nearly identical *p*-*i*-*n* solar cells: i) the first with *i*-region made from undoped GaAs (well material) and ii) the second with *i*-region from $Al_{0.1}Ga_{0.9}As$ (barrier material).

Keywords: solar cell, quantum well, optimisation, $A^{III}B^{V}$, GaAs, AlGaAs.

1. Introduction

Quantum wells (QWs) in solar cells (SCs) are employed to increase the efficiency of common *p*-*i*-*n* solar cells [1–3]. The absorption edge of a SC is determined by the width and depth of QWs. Higher photocurrent can be generated if wells are deeper, since longer wavelengths are then absorbed. The output voltage (open-circuit) depends on the barrier material band gap. Deeper wells increase photocurrent and decrease open-circuit voltage [2–5]. Wider wells decrease the absorption edge, more energy levels are available and absorption per one well rises in consequence [2]. Larger number of wells within the depletion region decreases the absorption edge and increases the photocurrent [2–5]. The number of QWs has an opposite effect on the output voltage than on the photocurrent [2, 6–8]. That leads to the conclusion that an increase in the efficiency is determined by the optimization of a SC design.

2. Device description

The basic *p*-*i*(MQW)-*n* structure is shown in Fig. 1. The n^+ GaAs:Si (doped at 1×10^{18} cm^{-3}) substrate (1) and buffer layer (2), 400 and 0.5 μm thick, were applied

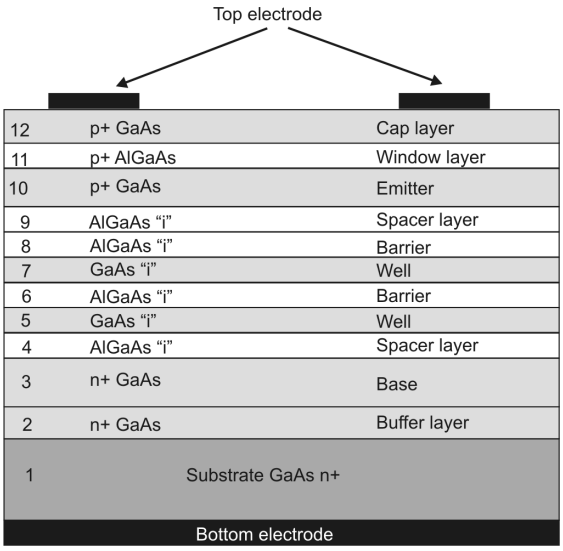

Fig. 1. Solar cell structure.

respectively. The *n*-type region (3), Si doped, and *p*-type region (10), Zn doped, were composed of GaAs. There are special separating layers (4, 9), GaAs QWs (5, 7) and $Al_xGa_{1-x}As$ barriers (6, 8) between the emitter (10) and the base (3). Spacers were made from intrinsic barrier material. On the top of the structure $Al_xGa_{1-x}As$ window layer (11) 0.08 μm wide was used. Window layer was followed by the GaAs cap layer (12). Two reference *p*-*i*-*n* structures were also taken: layers from 4 to 9 are made from undoped GaAs – *p*-*i*(GaAs)-*n* and undoped $Al_{0.1}Ga_{0.9}As$ – *p*-*i*($Al_{0.1}Ga_{0.9}As$)-*n*.

3. Device simulations

SimWindows version 1.5.0 was used to simulate devices under non-concentrated AM 1.5 spectrum with P_{in} in average equal to 1000 W/m^2. Well and barrier width, well depth with constant value of intrinsic region width, number of wells in the intrinsic region, doping concentration of *n*-region, width and doping concentration of *p*-region, width of separation layers and Al fraction in window layer were changed. Devices that reached the highest value of efficiency were classified to the next stage of optimization.

Simulation of devices with various well and barrier width was the first step. Different intrinsic region thicknesses were examined. Samples with various quantum width d_{qw} and barrier width d_b were simulated (Figs. 2 and 3).

T a b l e. Well and barrier dimensions in tested solar cells samples.

Sample	*A*	*B*	*C*	*D*	*E*	*F*	*G*	*H*	*I*	*J*	*K*
d_b [nm]	49	40	10	20	10	15	45	4	9	5	10
d_{qw} [nm]	1	10	10	5	15	10	5	1	1	5	5

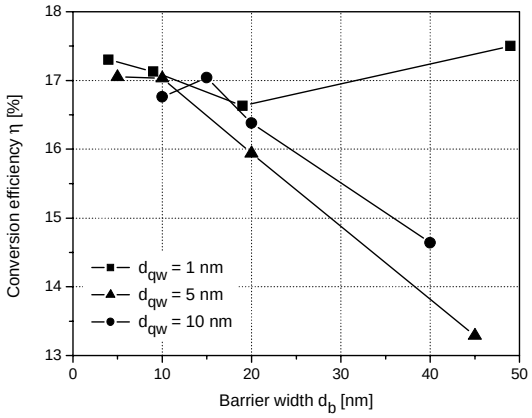

Fig. 2. Efficiency *vs.* barrier width at constant well width.

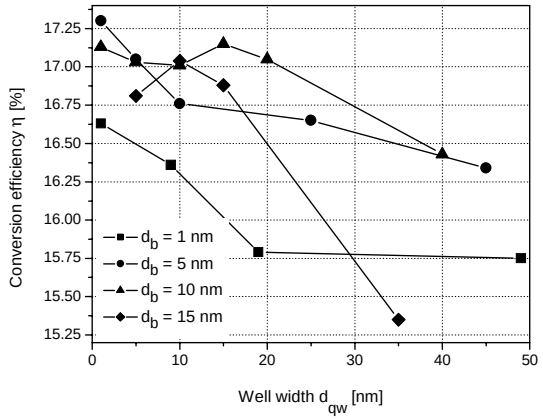

Fig. 3. Efficiency *vs.* well width at constant barrier width.

Details about well and barrier dimensions in samples that were chosen are given in the Table.

3.1. Well depth optimization

The depth of wells was regulated by changing the fraction of Al in barrier material. Two different *i*-region thicknesses were examined: 0.5 and 0.1 μm. The Al fraction was altered from 0.05 to 0.35. Results are shown in Figs. 4 and 5 for each *i*-region thickness, respectively.

The highest values of the efficiency for samples with 0.5 μm *i*-region thickness were obtained for 0.1 Al fraction in barrier material. The best efficiency was reached by sample *E*. This sample and three more: *A*, *B* and *G*, were chosen to the next simulations. There is a plot for *p*-*i*-*n* control sample with *i*-region made from $Al_xGa_{1-x}As$. This sample has also one of the best values of the efficiency.

For the samples, with 0.1 μm thick intrinsic region, the best efficiency was obtained for samples *K* and *J* for Al fraction equal to 0.1. The samples were taken to the next level of our optimization.

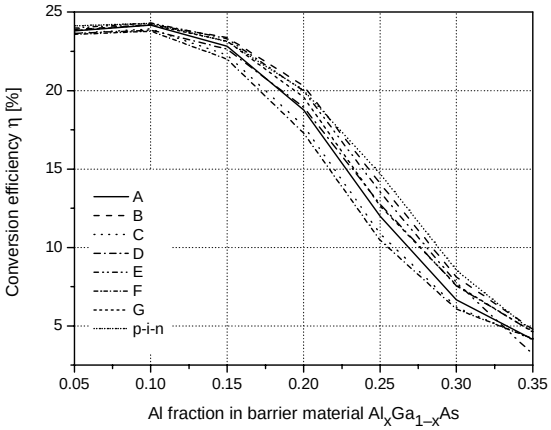

Fig. 4. Efficiency *vs.* Al fraction x in barrier material $Al_xGa_{1-x}As$ for intrinsic region width equal to 0.5 μm.

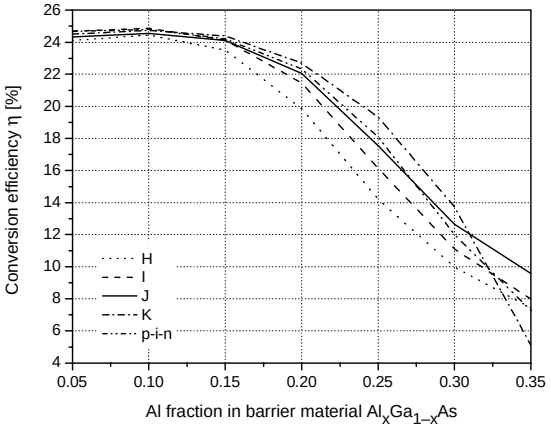

Fig. 5. Efficiency *vs.* well depth for intrinsic region width equal to 0.1 μm.

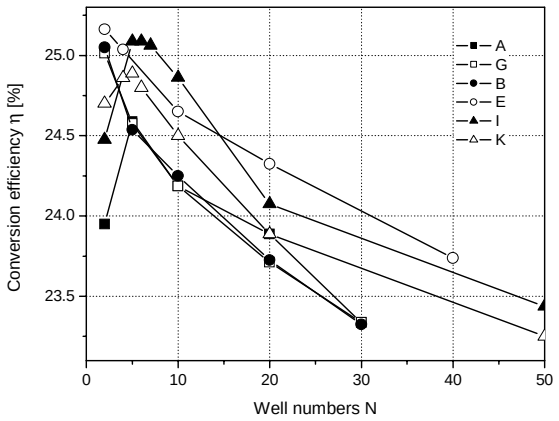

Fig. 6. Efficiency as a function of the wells quantity.

3.2. Well number optimization

The numbers of wells were varied from 2 to 30 or 50. The best efficiencies were obtained for two wells (Fig. 6) apart from cells *A*, *K* and *I* that had largest efficiency for five wells. The largest value of efficiency was achieved for sample *E* followed by samples *I*, *B* and *G*. All four samples have been classified to the next simulation.

3.3. Base doping concentration optimization

Doping concentration in base layer of samples *B*, *E*, *G* and *I* were optimized. Obtained results are depicted in Fig. 7. For comparison characteristics for *p-i-n* control samples were plotted. Reference samples had intrinsic layer width equal to the sum of widths of well and barrier layers. The best efficiency was obtained for *p-i*($Al_{0.1}Ga_{0.9}As$)-*n*

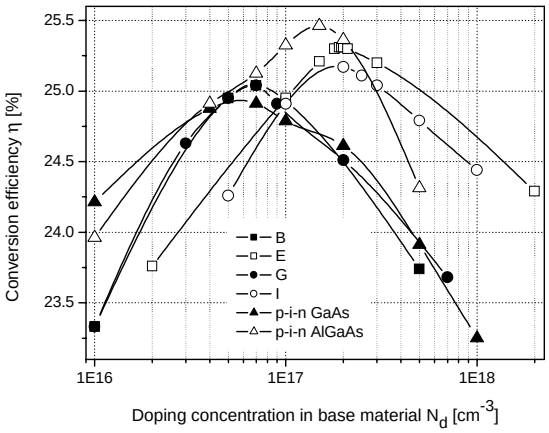

Fig. 7. Efficiency as a function of the doping concentration in base layer material.

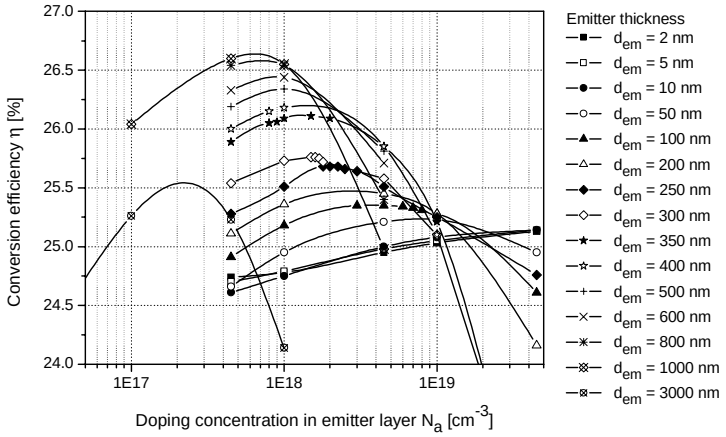

Fig. 8. Efficiency as a function of the doping concentration in emitter layer material (sample *E*).

solar cell. Among MQWSCs the largest efficiency was shown by samples *E* and *I* for base doping concentration $N_a = 2\times10^{17}$ cm^{-3}.

3.4. Emitter doping concentration optimization

Emitter, window layer and cap layer were doped identically. The width and doping concentration of emitter layer for *E* and *I* solar cells were changed. Effects for sample *E* were shown in Fig. 8. For sample *I* the characteristics are very similar. The 100 nm thickness and 4×10^{18} cm^{-3} doping emitter layer were chosen. Emitter layer had to be thin because of possible diffusion of doping into wells during high temperature growth technology. The special spacer layers 20 and 25 nm of $Al_{0.1}Ga_{0.9}As$ were added.

3.5. Aluminium fraction in window layer optimization

Aluminium fraction *x* in $Al_xGa_{1-x}As$ window layer for sample *E* was changed from 0.1 to 0.8 (Fig. 9). An increase in efficiency was caused by increasing Al fraction. The best efficiency (27.4%) was obtained for $x = 0.8$.

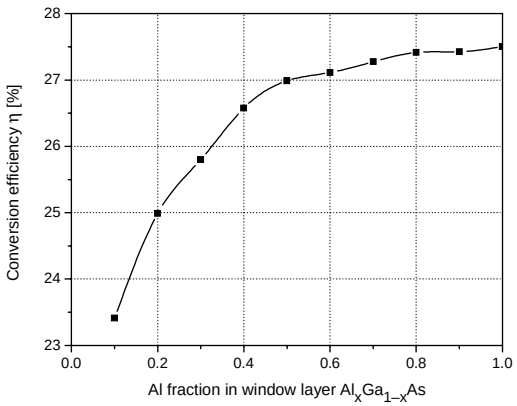

Fig. 9. Influence of Al fraction in window layer material (sample *E*) on the efficiency of MQWSC.

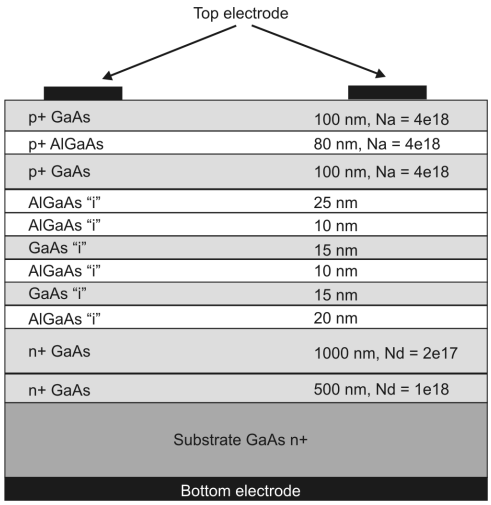

Fig. 10. Optimized structure of the MQW solar cell.

4. Results and discussion

Optimized structure of the MQW solar cell was depicted in Fig. 10. The device design with the highest value of efficiency contains two 15 nm wide GaAs wells and 10 nm wide $Al_{0.1}Ga_{0.9}As$ barriers. Two, 20 nm and 25 nm wide, $Al_{0.1}Ga_{0.9}As$ spacer layers, 100 nm wide (4×10^{18} cm^{-3} Zn-doped) emitter layer and 1000 nm (2×10^{17} cm^{-3} Si-doped) base layer were applied. Window layer was composed from $Al_{0.8}Ga_{0.2}As$. The cap layer application was required due to high contents of Al in window layer.

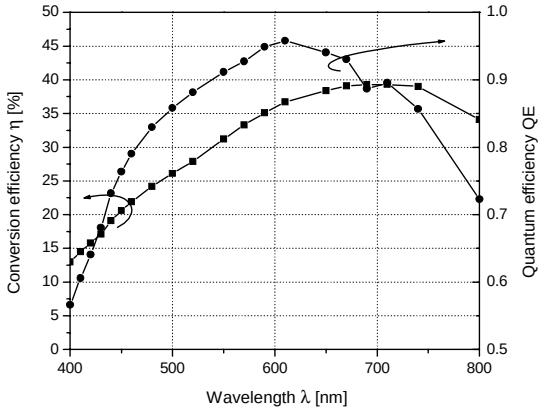

Fig. 11. Spectral characteristics for sample *E*.

Solar cells were simulated for wavelength from 400 to 800 nm in order to obtain spectral characteristics. The intensity of illumination for each wavelength was taken from AM 1.5 spectrum table (SimWindows 1.5.0. programme data). Values of conversion efficiency and external quantum efficiency for foreign wavelength were marked. Simulations for sample *E* were carried out. Results are shown in Fig. 11.

5. Conclusions

The 27.4% conversion efficiency was obtained by MQWSC. Efficiency of the control cells reached 26.6% and 27.5% for *p*-*i*(GaAs)-*n* and *p*-*i*($Al_{0.1}Ga_{0.9}As$)-*n*, respectively. The most important advantage of MQWSC is value of I_{max} being larger than for *p*-*i*-*n* control samples. The optimization algorithm described in the paper gave sufficiently good results.

Acknowledgments – This research was partially sponsored by the Polish Committee for Scientific Research under Grant No. PBZ 100/1/1/2004 and Wrocław University of Technology statutory grant.

References

[1] BARNHAM K.W.J., BUSHNELL D.B., CONNOLLY J.P., EKINS-DAUKES N., KLUFTINGER B.G., MAZZER M., NELSON J., *High efficiency III-V solar cells*, [In] *Proc. International School on Crystal Growth of Materials for Energy Production and Energy-saving Applications*, "Abdus Salam" International Centre for Theoretical Physics, Trieste, Italy, March 2001, p. 106.

[2] RIMADA J.C., HERNANDEZ L., *Modelling of ideal AlGaAs quantum well solar cells*, Microelectronics Journal **32**(9), 2001, pp. 719–23.
[3] BARNHAM K., BALLARD I., BARNES J., CONNOLLY J., GRIFFIN P., KLUFTINGER B., NELSON J., TSUI E., ZACHARIOU A., *Quantum well solar cells*, Applied Surface Sience **113/114**, 1997, pp. 722–33.
[4] BARNHAM K.W.J., DUGGAN G., *A new approach to high efficiency multi-band-gap solar cells*, Journal of Applied Physics **67**(7), 1990, pp. 3490–3.
[5] BARNHAM K., CONNOLLY J., GRIFFIN P., HAARPAINTNER G., NELSON J., TSUI E., ZACHARIOU A., OSBORNE J., BUTTON C., HILL G., HOPKINSON M., PATE M., ROBERTS J., FOXON T., *Voltage enhancement in quantum well solar cells*, Journal of Applied Physics **80**(2), 1996, pp. 1201–6.
[6] BARNHAM K.W.J., BALLARD I., CONNOLLY J.P., EKINS-DAUKES N.J., KLUFTINGER B.G., NELSON J., ROHR C., *Quantum well solar cells*, Physica E **14**(1-2), 2002, pp. 27–36.
[7] RAGAY F.W., MARTI A., ARA∨JO G.L., WOLTER J.H., *Experimental analysis of the efficiency of heterostructure GaAs/AlGaAs solar cells*, Solar Energy Materials and Solar Cells **40**(1), 1996, pp. 5–21.
[8] APERATHITIS E., VARONIDES A.C., SCOTT C.G., SAND D., FOUKARAKI V., ANDROULIDAKI M., HATZOPOULOS Z., PANAYOTATOS P., *Temperature dependence of photocurrent components on enhanced performance GaAs/AlGaAs multiple quantum well solar cells*, Solar Energy Materials and Solar Cells **70**(1), 2001, pp. 49–69.

Received June 6, 2005
in revised form November 6, 2005